This article has been accepted for publication in Journal of Lightwave Technology. This is the author's version which has not been fully edited and content may change prior to final publication. Citation information: DOI 10.1109/JLT.2026.3700386

Mach-Zehnder Interferometer Based on 3D Printed Microfiber Waveguide in C-shaped Fiber for Temperature and Refractive Index Measurement

Qipeng Huang, Liangyi Lin, Shanmei Zeng, Jingxian Cui, Lin Htein, Hwa-Yaw Tam, Xiaoyong Chen, Chuanxin Teng, Xuehao Hu and Hang Qu

***Abstract*—We report a compact in-line fiber Mach-Zehnder (M-Z) interferometer enabled by a femtosecond-laser two-photon-polymerization (TPP) printed microfiber in a C-shaped fiber. The C-shaped segment is fusion-spliced between two standard single-mode fibers, providing a mechanically robust platform, while the printed polymer microfiber bridges the two cores and supports multimode propagation to generate intermodal interference. The open cavity of the C-shaped fiber ensures strong evanescent-field interaction with the surrounding medium, resulting in high sensitivity. The device exhibits a high temperature sensitivity of 361 pm/°C and an air refractive-index sensitivity of 18300 nm/RIU. The sensor also demonstrates good stability and sub-second response. Compared with conventional tapered fiber M-Z interferometers, the proposed M-Z interferometer represents a promising and scalable solution for high-sensitivity, multi-parameter sensing, with potential applications in environmental monitoring, gas sensing, and biochemical detection.**

***Index Terms*— Mach-Zehnder interferometer, two photon polymerization, microfiber waveguide, optical fiber sensor.**

I. INTRODUCTION

AMONG manifold of fiber-optic interferometric sensors, the sensors using Mach-Zehnder (M-Z) interference modality have received tremendous interest in both academic and industrial fields, since they offer plenty of advantages such as straightforward sensing mechanism, ease of fabrication, relatively high sensitivity, and multiplexing capability [1]-[3]. A variety of M-Z fiber sensors have been proposed for sensing applications in temperature, strain, refractive index, air pressure, displacement, and biochemical reactions [4], [5].

In M-Z fiber sensors, guided light is first split into different optical paths or guided modes. Upon recombination, interference is generated. Variations in the measurand modulate the phase difference between the interfering beams, leading to changes in the output intensity or spectral shifts, which constitute the fundamental sensing mechanism of M-Z fiber sensors. The most common approach for fabricating in-line M-Z interferometers is to form a single taper or cascaded tapers using fiber fusion splicing or flame-brush techniques [4], [6], [7]. Owing to the strong light-matter interaction at the tapered regions, such structures can achieve high sensitivity. However, the intrinsic fragility of tapered fibers results in poor mechanical robustness, which significantly compromises device portability and practical applicability. Alternatively, single-mode-multimode-single-mode (SMS) fiber structures or single-mode fiber (SMF)-multicore fiber (MCF)-SMF configurations can also realize light splitting and recombination in M-Z fiber sensors [3], [8]-[10]. In these schemes, sensing relies on the interaction between the evanescent field of guided modes in the multimode fiber or MCF and the external environment, which inherently limits sensitivity. To enhance light-matter interaction, microholes or microfluidic channels can be introduced into the multimode fiber (MMF) or MCF using fs-laser micromachining [11], [12]. While effective, this approach further complicates the fabrication process. Photonic crystal fibers (PCFs) have also been employed as substitutes for multimode fibers [13]-[15]. Benefiting from the porous cladding structure, substances infiltrated into the air holes can exert a stronger influence on the guided modes, thereby improving sensitivity. Nevertheless, PCFs are generally expensive, and infiltration of aqueous samples into their micron-scale air holes is technically challenging and time-

This work was supported in part by National Natural Science Foundation of China (62475140); Natural Science Foundation of Guangxi Province (2023GXNSFDA026040); Guangxi Key Laboratory of Optoelectronic Information Processing (GD23203); the Dongguan Science and Technology of Social Development Program (20221800905082); Special projects in key fields of colleges and universities in Guangdong Province (2023ZDZX2063).
(Corresponding authors: Xuehao Hu; Hang Qu.)

Qipeng Huang, Liangyi Lin, Shanmei Zeng and Hang Qu are with the Department of Physics, Shantou University, Shantou 515063, China (e-mail: 23qphuang@stu.edu.cn; 23lylin@stu.edu.cn; 23smzeng@stu.edu.cn; haqux@stu.edu.cn).

Jingxian Cui, Lin Htein and Hwa-Yaw Tam are with the Department of Electrical and Electronic Engineering, The Hong Kong Polytechnic University, Kowloon, Hong Kong SAR 997700, China (e-mail: jing-xian.cui@polyu.edu.hk; htein.lin@polyu.edu.hk; hwa-yaw.tam@polyu.edu.hk).

Xiaoyong Chen is with the School of Electrical Engineering and Intelligentization, Dongguan University of Technology, Songshan Lake High-Tech Industrial Development Zone, Dongguan 523808, China (e-mail: xychen@dgut.edu.cn).

Chuanxin Teng is with the Guangxi Key Laboratory of Optoelectronic Information Processing, Guilin University of Electronic Technology, Guilin 541004, China (e-mail: cxteng@guet.edu.cn).

Xuehao Hu is with the Department of Electromagnetism and Telecommunication, University of Mons, Boulevard Dolez 31, 7000 Mons, Belgium (e-mail: xuehao.hu@umons.ac.be).

This article has been accepted for publication in Journal of Lightwave Technology. This is the author's version which has not been fully edited and content may change prior to final publication. Citation information: DOI 10.1109/JLT.2026.3700386

consuming due to the high flow resistance, which scales inversely with a fourth power of the pore diameter. Moreover, cascaded long-period gratings (LPGs) or laser-milled microcavities can be incorporated into SMFs to first couple the core mode into high-order cladding modes that interact with external perturbations [1], [16], and subsequently re-couple them back into the core to form an interferometer. Similar to SMS-based structures, the reliance on evanescent-field interactions of cladding modes ultimately constrains the achievable sensitivity of these devices.

Nowadays, femtosecond (fs) lasers featured by ultrashort pulse durations and extremely high peak powers have opened a revolutionary avenue for the fabrication of advanced optical devices, particularly in high-precision waveguide engineering [17]. A variety of approaches have been developed to fabricate waveguides within or on optical fibers, including direct fs-laser writing to locally modify the refractive index along predefined paths inside coreless fibers, as well as two-photon-polymerization (TPP) for printing three-dimensional waveguide structures on fiber tips. For instance, Liao et al. employed an fs-laser to inscribe two waveguides in a coreless fiber segment sandwiched between two SMFs, forming an in-line M-Z interferometric sensor for refractive-index measurement [18]. Using a similar configuration, Zhao et al. used similar structure along with a hollow-core fiber working as a Fabry-Perot cavity to realize simultaneous salinity and temperature sensing of seawater [19]. He et al. reported a single-mode helical Bragg grating waveguide (HBGW) written in a multimode coreless fiber. Owing to its unique helical geometry, the HBGW simultaneously functions as a depressed-cladding waveguide and produces strong Bragg resonance through its intrinsic periodicity [20]. The device exhibited temperature and strain sensitivities of 11.65 pm/°C and 1.29 pm/με, respectively. In parallel, fs-laser-based waveguide fabrication using TPP technology has developed rapidly in recent years and has been widely applied in life sciences, materials science, mechanics, and related fields [21]. As a high-resolution and highly flexible 3D printing technique, TPP enables efficient fabrication of micro-/nano-structures on fiber-optic platforms, showing excellent capability in realizing complex, high-performance optical, mechanical, and biological structures [22]-[24]. For example, Violakis et al. fabricated a waveguide coupler on the tip of a four-core optical fiber to enable efficient coupling to and from a single-core fiber, achieving an insertion loss below 5 dB [25]. Gill et al. printed a bus waveguide and a racetrack resonator on the facet of a dual-core fiber to excite whispering-gallery modes for temperature sensing [26]. Overall, these two fs-laser micromachining approaches, namely, direct laser writing and TPP-based fabrication, offer unprecedented design freedom and integration potential for next-generation fiber-optic photonic devices.

In this paper, we propose the fabrication of a microfiber waveguide inside a C-shaped fiber using fs-laser-assisted TPP 3D printing technique. The C-shaped fiber is fusion-spliced between two standard SMFs, forming an integrated in-line structure. Owing to the multimode propagation supported by the printed microfiber, the device inherently functions as a M-Z interferometer. The diameter of the printed microfiber can be as small as ~2 μm. The C-shaped fiber simultaneously serves as the mechanical support of the M-Z interferometer and as an open sensing reservoir for gaseous or liquid analytes. To demonstrate proof-of-principle applications, the proposed device is employed for sensing of refractive index (pressure) of air and temperature, achieving the sensitivities of ~18300 nm/RIU (~55 pm/kPa) and ~361 pm/°C, respectively.

The proposed M-Z fiber structure and its fabrication strategy offer several distinct advantages. 1) The fs-laser TPP-based approach enables precise and flexible control over the length and diameter of the microfiber waveguide, allowing the fabrication of M-Z interferometers with well-defined geometrical parameters. This, in turn, facilitates efficient spectral modulation and high sensing sensitivity, primarily attributed to the strong evanescent-field leakage and thus strong light-matter interaction within the submicron-scale microfiber segment. 2) Compared to the fiber tapers drawn by flame-brush technique, the proposed M-Z structure supported by C-shaped fiber has superior mechanical strength and thus improved practical applicability. 3) The C-shaped fiber geometry provides an open and well-defined interaction region, enabling direct and efficient exposure of the microfiber waveguide to external gaseous or liquid samples. Moreover, only a small amount of analyte is required to fill the C-shaped cavity, which is beneficial for biosensing. 4) The printed microfiber could be further decorated with functionalized layers responsive to a variety of analytes. Alternatively, functionalized particles may also be doped in the printing resins, potentially improving the sensor versatility. 5) Owing to the flexibility of the fs-laser TPP 3D printing process, the proposed approach is readily extendable to the fabrication of more complex interferometric architectures, such as multi-arm M-Z structures or cascaded interferometers.

II. SENSING PRINCIPLE

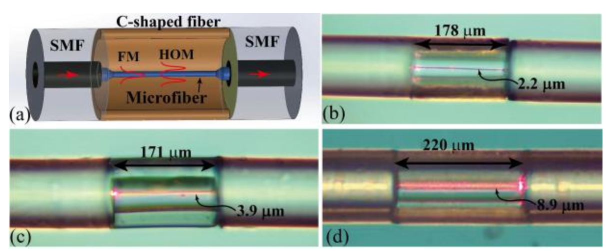

Fig. 1. (a) Schematic diagram of the 3D structure; (b-d) three fabricated samples of the M-Z fiber interferometers with the microfibers fabricated in different lengths and diameters.

The working principle of the sensor can be explained as follows. As shown in Fig. 1(a), when light enters microfiber inside the C-shaped fiber region from the input SMF, the fundamental mode (FM) is primarily coupled into the microfiber through a 3D printed gradient region. Due to multimode property of the microfiber, some higher-order modes (HOMs) with a large fraction of evanescent field in the air are also excited. Via another gradient region on the other side of the microfiber, both the FM

This article has been accepted for publication in Journal of Lightwave Technology. This is the author's version which has not been fully edited and content may change prior to final publication. Citation information: DOI 10.1109/JLT.2026.3700386

and HOMs are recoupled into the SMF at the output end, thus generating an interferent spectrum. In this M-Z interferometer, the output intensity of light is typically presented by the following Eqs. (1)-(4):

$$I = I_1 + I_2 + 2\sqrt{I_1 I_2 cos\Phi} \tag{1}$$

where I_1 and I_2 represent the intensity of the FM and the HOM, respectively. The intensity I of the optical output depends on the phase difference between the modes involved in the interference, which is expressed as:

$$\Phi=\frac{2\pi}{\lambda}(\Delta n_{\mathrm{eff}})L=\frac{2\pi}{\lambda}\left(n_{\mathrm{FM,\ eff}}-n_{\mathrm{HOM,\ eff}}\right)L \tag{2}$$

where L is length of the microfiber, λ is the wavelength of light in free space, and Δn_{eff} represents the difference of the effective refractive index between the FM and the HOMs. According to Eqs. (2), the resonant wavelength (λ_{peak}) in the output spectrum can be expressed as:

$$\lambda_{\mathrm{peak}}=\frac{\Delta n_{\mathrm{eff}}L}{m} \tag{3}$$

where m is a positive integer. Changes in analytes would then modulate Δn_{eff}, thus leading to shift of the resonant peak in the output spectrum, which constitutes the general sensing mechanism of the M-Z interferometer. The free spectral range of the devices could be approximated as:

$$FSR=\frac{\lambda_m^2}{\Delta n_{\mathrm{eff}}L} \tag{4}$$

III. EXPERIMENT

A. Fabrication of M-Z Fiber Interferometers

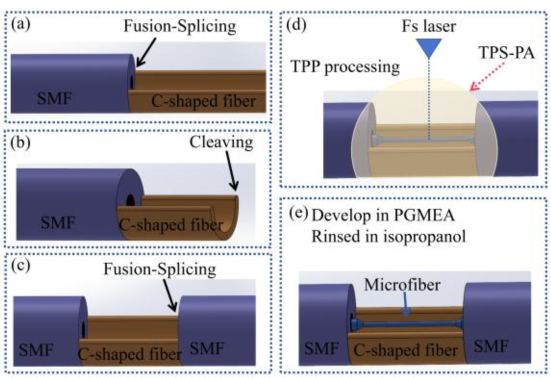

Fig. 2. Schematic of the fabrication process of the fiber M-Z interferometer

To fabricate the M-Z interferometer experimentally, a standard SMF (core diameter: 8.2 μm, cladding diameter: 125 μm) was first spliced to a segment of C-shaped fiber using a fusion splicer (FSM-100P, Fujikura), which is demonstrated in Fig. 2(a). The C-shaped fiber, custom-fabricated by our collaborators at Hong Kong Polytechnic University, had an outer diameter of ~125 μm and an inner diameter of ~70 μm. To fabricate this fiber, a pure silica tube with an inner diameter of 4 mm and outer diameter of 12 mm is machined to create a lateral slot along the axial direction, resulting in a C-shaped preform. Then the preform is drawn into the C-shaped fiber in a commercial fiber drawing tower (NEXTROM OFC20). During the fiber drawing process, the oven of the tower was set to a relatively low temperature of 1890 °C to maintain the cross-sectional shape of the fiber [27]. Also note that Splicing the C-shaped fiber to standard SMF requires careful optimization of the fusion parameters. In our experiment, a discharge time of 500 ms and a current of approximately 16 mA were used to achieve stable splicing. During the process, the fusion point is intentionally offset by ~200 μm toward the SMF side to avoid collapse of the C-shaped structure. After the initial splicing, the free end of the C-shaped fiber was then cleaved to a designated length using a fiber cleaver (CT50, Fujikura) under optical microscope observation as shown in Fig. 2(b). Subsequently, the free end of the C-shaped fiber was fusion-spliced to another standard SMF, forming a mechanically robust in-line structure (Fig. 2(c)). The assembled structure was then mounted on a six-axis motorized stage in a fs-laser μFAB Microfabrication Workstation (Newport). Note that the opening of the C-shaped fiber was oriented upward by a rotary fiber clamp to ensure proper laser access during fabrication. A negative photoresist (TPS-PA, Omeda) was applied to fully immerse the C-shaped fiber region. The fs-laser beam was tightly focused via a 63× immersion objective, and TPP was induced by scanning the laser along a predefined trajectory (Fig. 2(d)). In this manner, a polymer microfiber was directly printed to connect the cores of the two SMFs across the C-shaped fiber segment, thereby forming the M-Z interferometer. The quality of the printed microfiber strongly depends on the laser processing parameters, including pulse energy, repetition rate, and scanning speed, which were optimized to 5.94 nJ, 5 kHz, and 0.2 mm/s, respectively. After the 3D printing process, the entire structure is immersed in propylene glycol monomethyl ether acetate (PGMEA) developer for 5-10 minutes, depending on the diameter of the printed microfiber, to remove unpolymerized resin. It is then rinsed in isopropanol for ~3 minutes to complete the cleaning process (Fig. 2(e)). We demonstrated several experimental samples with different lengths and diameters of the microfibers in the C-shaped fiber in Fig. 1(b-d). To visualize the microfiber guidance, we coupled light from a red laser into the core of the input SMF. Also note that to facilitate a stable connection of the microfiber to the SMF, we printed a 10-μm-long taper (gradient region) at each extremity of the microfiber shown in Fig. 1(b, c). The diameter of the taper increased from the waist diameter (which are ~2.2 μm and ~3.9 μm, respectively) of the microfiber to ~7 μm at the interface of the SMF. In the following, we used the M-Z interferometer with a microfiber diameter of 2.2 μm to demonstrate its proof-of-principle applications in sensing of gas refractive index (pressure) and environment temperature. All subsequent measurements are performed using this sensor device.

B. Air Refractive Index/Pressure Sensing Characterization

As shown in Fig. 3, in the pneumatic characterization experiment, light from the spectral interrogator (HBK, FS22SI) was directed from port CH1 through the sample's input section via an SMF. The output light from the sample was then sent to a fiber circulator (port 1 to port 2) and finally to port CH2 of the interrogator, allowing for direct analysis of the transmission spectrum. The sensor probe was placed inside a vacuum drying oven (DZF-6020, KJ Group Inc.) with a built-in pressure gauge

This article has been accepted for publication in Journal of Lightwave Technology. This is the author's version which has not been fully edited and
content may change prior to final publication. Citation information: DOI 10.1109/JLT.2026.3700386

and a temperature controller, which enabled a gradual reduction of the internal pressure from approximately 100 kPa (standard atmospheric pressure) to 30 kPa in steps of 10 kPa at a constant temperature of 20 °C. Under these conditions, the corresponding refractive index of air decreased from 1.0003 to 1.00009 [28], with a decremental change of ~3×10^{-5} per pressure step.

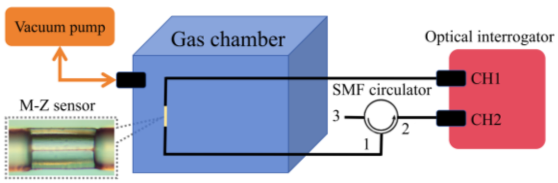

Fig. 3. Schematic diagram of the air pressure test setup.

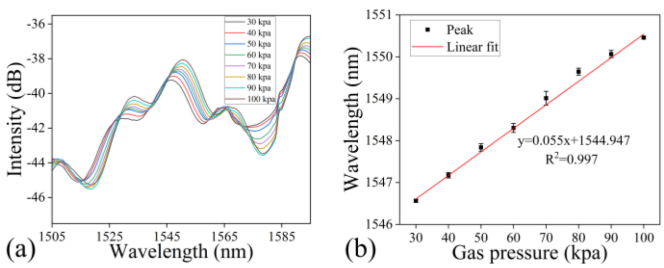

Fig. 4. For the barometric detection of the sensing structure, (a) is the peak drift, and (b) is the fitting curve with error bars.

As the air pressure (and hence the refractive index) increases, the transmission spectrum exhibits a pronounced red shift, as shown in Fig. 4(a). Fig. 4(b) presents the linear fitting of the interference peak wavelength shift as a function of pressure, with error bars derived from five repeated measurements at each pressure point. From the linear regression, the pressure sensitivity is determined to be 55 pm/kPa, corresponding to a refractive-index sensitivity of 18,300 nm/RIU. This sensitivity is one to three orders of magnitude higher than that of conventional M-Z sensors based on SMS structures or fiber gratings [29], [30] and is comparable to the most sensitive microfiber-based M-Z interferometric sensors reported to date [31], [32]. The stability of the sensor under varying pressure conditions was also evaluated, as shown in Fig. 5. The transmission spectra were continuously monitored for 420 s at pressure levels of 50 kPa and 90 kPa, with a sampling interval of 10 s. The standard deviations in the measurements were 59.3 pm at 50 kPa and 70.7 pm at 90 kPa, respectively. During the measurement period, the fluctuation of the resonance wavelength remained within ±200 pm, indicating good stability of the sensor.

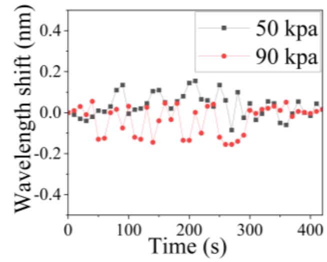

Fig. 5. Stability of air pressure measurement.

C. Temperature Sensing Characterization

For experimental characterization of the temperature-sensing performance, the sensing probe was placed on a temperature-controlled breadboard (PTC1, Thorlabs), and the transmission spectra were recorded while the temperature was varied from 25 °C to 45 °C in steps of 2 °C. The interference spectrum undergoes a blue shift as the temperature increases, as shown in Fig. 6(a).

It is worth mentioning that the temperature measurement was conducted with an interval of approximately two weeks after the air refractive index/pressure measurement, which led to slight spectral variations. These differences can be attributed to minor environmental and experimental factors, such as fluctuations in ambient conditions (e.g., humidity and temperature), slight changes in fiber alignment or coupling conditions, and potential aging or stress relaxation of the polymer microfiber, all of which may induce small baseline shifts in the interference spectrum without affecting the overall sensing performance.

The linear fitting of the interference peak wavelength as a function of temperature is presented in Fig. 6(b), where the error bars are derived from five repeated measurements at each temperature point. Based on the linear regression, the temperature sensitivity of the sensor is determined to be -361 pm/°C.

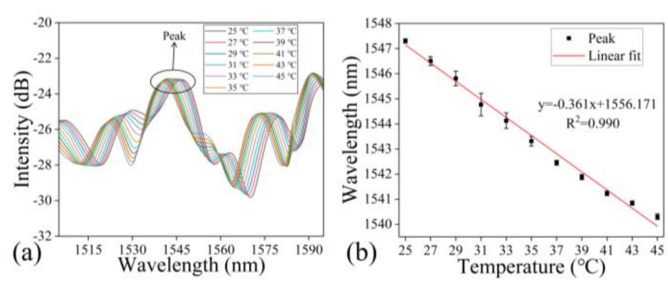

Fig. 6. For the temperature detection of the sensing structure, (a) is the peak drift, and (b) is the fitting curve with error bars.

The real-time response of the sensor to temperature variations was further investigated to evaluate its response time, as shown in Fig. 7(a). The red curve represents the temperature evolution of the breadboard, as it was increased from 25 °C to 27 °C. After the temperature setpoint was changed, the breadboard underwent a proportional-integral-derivative (PID) control process and gradually stabilized within approximately 50 s. During this process, transmission spectra were recorded at

This article has been accepted for publication in Journal of Lightwave Technology. This is the author's version which has not been fully edited and content may change prior to final publication. Citation information: DOI 10.1109/JLT.2026.3700386

a sampling rate of 1 Hz. Based on the temporal evolution of the interference peak wavelength, the response time of the sensor was estimated to be less than 1 s. We also measured the stability of the sensor for temperature detection. As shown in Fig. 7(b), after the temperature stabilizes, the spectra were recorded every 10 seconds until 300 seconds, while the temperature of the breadboard was kept at 27 °C. The standard derivation in this measurement is 33.7 pm. The perturbation of the resonance wavelength is within the range of ±80 pm.

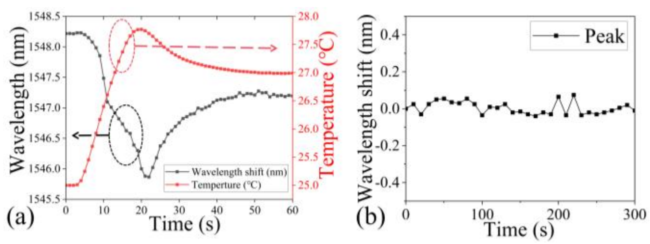

Fig. 7. Response time and stability test. The red dot in (a) is the real-time temperature change of the temperature-controlled breadboard, the black dot is the drift corresponding to the peak, and (b) is the stability of the temperature test.

The small spectral fluctuations observed during the pressure and temperature stability tests could be mainly attributed to residual environmental perturbations, particularly slight temperature drift, which induces changes in the effective refractive index through thermo-optic effects. In addition, minor stress relaxation of the polymer microfiber may also contribute to variations in the interference condition, resulting in small spectral fluctuations.

Table 1. Summary of performance of M-Z fiber sensors for sensing applications of temperature.

M-Z structure for temperature sensing	Temperature range (°C)	Sensitivity (pm/°C)	Ref.
Cascaded fiber tapers immersed in thermally responsive liquids	5-19	1950	[6]
SMF-FCF (four core fiber)-SMF structure	0-50	209	[8]
SMF-MMF-FMF (few mode fiber)-MMF-SMF structure	0-250	61.4	[33]
Parallel SMF-MMF structure with two fusion junctions	30-70	212	[34]
SMF-MMF-DCF (dual core fiber)-MMF-SMF structure with thermally responsive liquid filled in the microfluidic channel of the DCF	15-40	1420	[35]
SMF-NCF (no core fiber)-SMF structure with rubber coating	30-75 °C	253.75	[36]
Offset-spliced SMF-NCF-SMF structure immersed in thermally responsive liquid	30-36	5357.4	[37]
SMF-DF (D-shaped fiber)-SMF structure immersed various standard index-matched liquids with different refractive indices	34.1-37.9	84720	[38]
Optical microfiber mode interferometer embedded in a polymer with high thermo-optic coefficient	20-48	3101.8	[39]
3D printed microfiber waveguide in C-shaped fiber	25-45	361	This work

Table 2. Summary of performance of M-Z fiber sensors for sensing applications of air pressure.

M-Z structure for air pressure sensing	Air pressure range (kPa)	Sensitivity (pm/kPa)	Ref.
SMF-DCF-SMF structure with a fluidic channel transversely drilled through one core of the dual-core fiber	0-2000	9.6	[11]
SMF-CF (capillary fiber)-SMF structure based on the CF with microholes covered by photoresist diaphragm	0-35	1270	[40]
Tapered fiber with an air cavity	0-1000	12.967	[41]
Micro-air-cavity in SMF fabricated by fs-laser machining and fusion splicing	0-800	8.239	[42]
Two SMF-PCF (photonic crystal fiber)-SMF structures in parallel with a microchannel drilled in one of the PCF	0-80	2390	[43]
3D printed microfiber waveguide in C-shaped fiber	30-100	55	This work

The sensitivities of the proposed sensor are compared with those reported in previous literature, as summarized in Tables 1 and 2. We note that the temperature sensitivity of this sensor is generally higher than that of the M-Z interferometers based on the SMF-MMF-SMF structures, SMF-MCF-SMF, or cascaded tapers (or microcavities)[8], [10], but one or two orders smaller than that of the counterparts in which one path of the M-Z interferometer (e.g., SMF-D-fiber-SMF M-Z sensor) has complete overlap with thermal-responsive liquid/polymer [38]. To further improve the sensitivity, we may fill the C-shaped cavity with thermally sensitive liquids or polymer (such as PDMS) as demonstrated in Ref. [39]. As to sensing applications of air pressure, the sensitivity of the proposed sensor is higher than the counterparts reported in Ref. [41], [42], owing to the greater modal overlap with the air in the C-shaped fiber. However, to further enhance the sensitivity, one has to increase the effective sensing length by printing the microfiber in a longer in the C-shaped fiber. Also note that other functionalized materials (such as ZnO for humidity sensing or Pd for H_2 sensing) potentially may be deposited on the microfiber to realize sensing of a variety of analytes, thus promoting its versatility [44], [45].

Finally, we also would like to discuss the long-term stability of the sensor. The proposed microfiber is fabricated using a photoresist mainly consisting of polyester acrylate. Therefore, its long-term stability could be considerably affected by environmental factors such as moisture and oxygen. Due to the presence of ester groups, polyester acrylate can absorb water.

Moisture absorption may lead to swelling, refractive-index variation, reduced elastic modulus, and weakened interfacial adhesion. In extreme cases, this may result in polymer chain scission, reduced mechanical strength, or increased optical loss. Moreover, oxygen in air can also contribute to oxidative aging of polyester acrylate, particularly under elevated temperature or illumination. Oxidation may cause chain scission or changes in the crosslinked network. As a result, the material may become harder and more brittle, with reduced elasticity and possible formation of surface microcracks. The factors mentioned above may raise concerns for the long-term stability of the proposed sensor. While study of the long-term stability is beyond the scope of this paper, we note that the proposed structure should be kept in consistent environment such as in dry cabinet filled with inert gas for long-term storage and usage.

IV. Conclusion

In this work, we have demonstrated a compact and mechanically robust in-line M-Z interferometric fiber sensor based on a fs-laser TPP printed microfiber waveguide embedded in a C-shaped fiber. The printed microfiber bridges two SMFs and supports multimode propagation, enabling stable M-Z interference without relying on fragile tapered structures. Benefiting from the strong evanescent-field interaction of the micron-scale microfiber and the open geometry of the C-shaped fiber, the proposed sensor exhibits high sensitivity to both air refractive index (pressure) and temperature. Experimental results show a pressure sensitivity of 55 pm/kPa, corresponding to an ultrahigh refractive-index sensitivity of 18,300 nm/RIU, as well as a temperature sensitivity of 361 pm/°C. In addition, the device demonstrates good stability, fast response, and repeatable performance under both pressure and temperature variations. Compared with conventional M-Z interferometers based on fiber tapers, the proposed architecture offers several advantages, including enhanced mechanical strength, compact footprint, and an open sensing cavity that allows direct interaction with gaseous or liquid analytes. Furthermore, the high flexibility of the TPP-based fabrication approach enables precise control over the microfiber geometry and provides a versatile platform for further functionalization, such as coating or doping with responsive materials to extend sensing capabilities. Overall, the proposed M-Z interferometer represents a promising and scalable solution for high-sensitivity, multi-parameter fiber-optic sensing, with potential applications in environmental monitoring, gas sensing, and biochemical detection.

References

[1] Y. Zhao, H. Zhao, R.-q. Lv, and J. Zhao, "Review of optical fiber Mach–Zehnder interferometers with micro-cavity fabricated by femtosecond laser and sensing applications," Opt. Lasers Eng., vol. 117, pp. 7-20, 2019.
[2] Z. Wen, Z. Guan, J. Dong, H. Li, Y. Cai, and S. Gao, "A review of sensitivity enhancement in interferometer-based fiber sensors," Sens., vol. 22, no. 7, p. 2506, 2022.
[3] K. Wang, X. Dong, M. H. Köhler, P. Kienle, Q. Bian, M. Jakobi, and A. W. Koch, "Advances in optical fiber sensors based on multimode interference (MMI): a review," IEEE Sens. J., vol. 21, no. 1, pp. 132-142, 2020.
[4] V. Bhardwaj, K. Kishor, and A. C. Sharma, "Tapered optical fiber geometries and sensing applications based on Mach-Zehnder Interferometer: A review," Opt. Fiber Technol., vol. 58, p. 102302, 2020.
[5] Y. Wei, T. Jiang, C. Liu, X. Zhao, L. Li, R. Wang, C. Shi, and C. Liu, "Sawtooth fiber MZ vector bending sensor available for multi parameter measurement," J. Lightwave Technol., vol. 40, no. 17, pp. 6037-6044, 2022.
[6] S. Liu, Y. Wang, T. Xie, S. Zheng, H. Wang, and H. Fu, "Highly sensitive optical fiber temperature sensor based on Mach-Zehnder modal interferometer with taper structure," Opt. Commun., vol. 582, p. 131640, 2025.
[7] L. Zhang, W. Zhang, L. Chen, T. Yan, L. Wang, B. Wang, and Q. Zhou, "A fiber bending vector sensor based on M–Z interferometer exploiting two hump-shaped tapers," IEEE Photonics Technol. Lett., vol. 27, no. 11, pp. 1240-1243, 2015.
[8] C. Li, T. Ning, C. Zhang, J. Li, C. Zhang, X. Wen, H. Lin, and L. Pei, "All-fiber multipath Mach-Zehnder interferometer based on a four-core fiber for sensing applications," Sensor Actuat A-phys, vol. 248, pp. 148-154, 2016.
[9] P. Hu, Z. Chen, M. Yang, J. Yang, and C. Zhong, "Highly sensitive liquid-sealed multimode fiber interferometric temperature sensor," Sensor Actuat A-phys, vol. 223, pp. 114-118, 2015.
[10] D. Yi, Z. Huo, Y. Geng, X. Li, and X. Hong, "PDMS-coated no-core fiber interferometer with enhanced sensitivity for temperature monitoring applications,"Opt. Fiber Technol., vol. 57, p. 102185, 2020.
[11] Z. Li, C. Liao, Y. Wang, L. Xu, D. Wang, X. Dong, S. Liu, Q. Wang, K. Yang, and J. Zhou, "Highly-sensitive gas pressure sensor using twin-core fiber based in-line Mach-Zehnder interferometer," Opt. Express, vol. 23, no. 5, pp. 6673-6678, 2015.
[12] C. Zhao, H. Qiu, H. Chen, X. Hu, Q. Yu, Z. Lian, J. Li, H. Qu, "In-fiber Mach-Zehnder temperature sensor using silicone-oil-filled duel core fiber," Sensor Actuat A-phys., vol. 323, pp. 112633, 2021.
[13] N. L. Andrews, R. Ross, D. Munzke, C. van Hoorn, A. Brzezinski, J. A. Barnes, O. Reich, and H.-P. Loock, "In-fiber Mach-Zehnder interferometer for gas refractive index measurements based on a hollow-core photonic crystal fiber," Opt. Express, vol. 24, no. 13, pp. 14086-14099, 2016.
[14] I. Shavrin, S. Novotny, A. Shevchenko, and H. Ludvigsen, "Gas refractometry using a hollow-core photonic bandgap fiber in a Mach-Zehnder-type interferometer," Appl. Phys. Lett., vol. 100, no. 5, 2012.
[15] F. Ahmed, V. Ahsani, K. Nazeri, E. Marzband, C. Bradley, E. Toyserkani, and M. B. Jun, "Monitoring of carbon dioxide using hollow-core photonic crystal fiber Mach–Zehnder interferometer," Sens., vol. 19, no. 15, p. 3357, 2019.
[16] J. Fu, C. Guan, Z. Zhu, M. Wang, P. Huang, P. Li, J. Shi, and L. Yuan, "In-fiber M-Z interferometer based on cascaded long period gratings in embedded-core fiber," IEEE Photonics Technol. Lett., vol. 29, no. 21, pp. 1876-1879, 2017.
[17] B. Zhang, W. Yan, and F. Chen, "Recent advances in femtosecond laser direct writing of three-dimensional periodic photonic structures in transparent materials," Adv. Photonics, vol. 7, no. 3, p. 034002, 2025.
[18] Y. Zhang, C. Lin, C. Liao, K. Yang, Z. Li, and Y. Wang, "Femtosecond laser-inscribed fiber interface Mach–Zehnder interferometer for temperature-insensitive refractive index measurement," Opt. Lett., vol. 43, no. 18, pp. 4421-4424, 2018.
[19] Y. Zhao, J. Zhao, X. Wang, Y. Peng, and X. Hu, "Femtosecond laser-inscribed fiber-optic sensor for seawater salinity and temperature measurements," Sens. Actuators B Chem., vol. 353, p. 131134, 2022.
[20] J. He, J. He, X. Xu, B. Du, B. Xu, C. Liao, Z. Bai, and Y. Wang, "Single-mode helical Bragg grating waveguide created in a multimode coreless fiber by femtosecond laser direct writing," Photonics Res., vol. 9, no. 10, pp. 2052-2059, 2021.
[21] C. Xiong, C. Liao, Z. Li, K. Yang, M. Zhu, Y. Zhao, and Y. Wang, "Optical fiber integrated functional micro-/nanostructure induced by two-photon polymerization," Front. Mater., vol. 7, p. 586496, 2020.
[22] H. Wei, Z. Wu, K. Sun, H. Zhang, C. Wang, K. Wang, T. Yang, F. Pang, X. Zhang, and T. Wang, "Two-photon 3D printed spring-based Fabry–Pérot cavity resonator for acoustic wave detection and imaging," Photonics Res., vol. 11, no. 5, pp. 780-786, 2023.
[23] Y. Liu, R. Zheng, S. Peng, Z. Xin, G. Xu, H. Wei, C. Caucheteur, X. Hu, and H. Qu, "Highly sensitive fiber-optic Fabry-Perot microforce probe," J. Lightwave Technol., vol. 43, no. 1, pp. 383-389, 2025.
[24] F. Wang, C. Liao, M. Zou, D. Liu, H. Huang, C. Liu, and Y. Wang, "Microstructured cantilever probe on optical fiber tip for microforce sensor," Photonic Sens., vol. 14, no. 2, p. 240204, 2024.

[25]G. Violakis, E. Athanasaki, S. Kostakis, N. Tiriakidis, K. Tiriakidis, T. Tiriakidou, and P. Polygerinos, "Single-to-four core optical fiber coupling using a two-photon polymerization produced waveguide," Opt. Express, vol. 32, no. 8, pp. 14240-14251, 2024.

[26]P. K. Gill, A. Kukin, and D. M. Marom, "Direct 3D-printed ring-resonator photonic circuit on a dual core fiber tip for remote sensing applications," Opt. Lett., vol. 49, no. 14, pp. 3946-3949, 2024.

[27]C. Wu, Z. Liu, A. Zhang, B. Guan, and H.-Y. Tam, "In-line open-cavity Fabry–Pérot interferometer formed by C-shaped fiber for temperature-insensitive refractive index sensing," Opt. Express, vol. 22, no. 18, pp. 21757-21766, 2014.

[28]M. Quan, J. Tian, and Y. Yao, "Ultra-high sensitivity Fabry–Perot interferometer gas refractive index fiber sensor based on photonic crystal fiber and Vernier effect," Opt. Lett., vol. 40, no. 21, pp. 4891-4894, 2015.

[29]Y. Cardona-Maya, I. Del Villar, A. B. Socorro, J. M. Corres, I. R. Matias, and J. F. Botero-Cadavid, "Wavelength and phase detection based SMS fiber sensors optimized with etching and nanodeposition," J. Lightwave Technol., vol. 35, no. 17, pp. 3743-3749, 2017.

[30]X. Wang, J. Zhang, K. Tian, S. Wang, L. Yuan, E. Lewis, G. Farrell, and P. Wang, "Investigation of a novel SMS fiber based planar multimode waveguide and its sensing performance," Opt. Express, vol. 26, no. 20, pp. 26534-26543, 2018.

[31]H. Luo, Q. Sun, X. Li, Z. Yan, Y. Li, D. Liu, and L. Zhang, "Refractive index sensitivity characteristics near the dispersion turning point of the multimode microfiber-based Mach–Zehnder interferometer," Opt. Lett., vol. 40, no. 21, pp. 5042-5045, 2015.

[32]D. Guo, L. Wu, H. Yu, A. Zhou, Q. Li, F. Mumtaz, C. Du, and W. Hu, "Tapered multicore fiber interferometer for refractive index sensing with graphene enhancement," Appl. Opt., vol. 59, no. 13, pp. 3927-3932, 2020.

[33]M. Liu, C. Ma, Y. Zhang, Q. Liu, H. Hu, and J. Wu, "Fiber optic high temperature sensor with weak strain sensitivity based on Mach-Zehnder interferometric structure," Optoelectron. Lett., vol. 21, no. 4, pp. 199-204, 2025.

[34]Y. Wu, Y. Liu, H. Zhuang, J. Cao, Y. Yang, X. Zhu, D. Sun, Y. Shi, and R. Tao, "High-Sensitivity Curvature Fiber Sensor Based on Miniature Two-Path Mach–Zehnder Interferometer," Micromachines-Basel, vol. 15, no. 8, p. 963, 2024.

[35]H. Chen, X. Hu, X. Chen, Q. Yu, Z. Lian, H. Wang, and H. Qu, "In-Line Interferometric Temperature Sensor Based on Dual-Core Fiber," IEEE Sens. J., vol. 21, no. 10, pp. 12146-12152, 2021.

[36]V. Bhardway, R. Gangwar, and V. Singh, "Silicone rubber-coated highly sensitive optical fiber sensor for temperature measurement," Opt. Engineering, vol. 55, no. 12, pp. 126107, 2016.

[37]X. Li, H. Wang, X. Chen, Q. Zhang, X. Chen, X. Zhou, X. Yan, Y. Zhao, and T. Cheng, "High-sensitivity Mach–Zehnder interferometer temperature sensor based on a no-core optical fiber with a large lateral offset," Appl. Opt., vol. 64, no. 16, pp. 4639-4645, 2025.

[38]H. Zhang, S. Gao, Y. Luo, Z. Chen, S. Xiong, L. Wan, X. Huang, B. Huang, Y. Feng, and M. He, "Ultrasensitive Mach-Zehnder interferometric temperature sensor based on liquid-filled D-shaped fiber cavity," Sens., vol. 18, no. 4, p. 1239, 2018.

[39]I. Hernández-Romano, D. Monzón-Hernández, C. Moreno-Hernández, D. Moreno-Hernandez, and J. Villatoro, "Highly sensitive temperature sensor based on a polymer-coated microfiber interferometer," IEEE Photonics Technol. Lett., vol. 27, no. 24, pp. 2591-2594, 2015.

[40]M. Yang, Y. Zhu, and J. Ren, "Hourglass-Shaped Fiber-Optic Mach-Zehnder interferometer for pressure sensing," Opt. Fiber Technol., vol. 84, p. 103746, 2024.

[41]C. Sun, F. Yu, H. Chen, D. Wang, and B. Xu, "Highly Sensitive Gas Pressure Sensing with Temperature Monitoring Using a Slightly Tapered Fiber with an Inner Micro-Cavity and a Micro-Channel," Sens., vol. 24, no. 21, p. 6844, 2024.

[42]W. Talataisong, D. N. Wang, R. Chitaree, C. R. Liao, and C. Wang, "Fiber in-line Mach–Zehnder interferometer based on an inner air-cavity for high-pressure sensing," Opt. Lett., vol. 40, no. 7, pp. 1220-1222, 2015.

[43]C. Mao, B. Huang, Y. Wang, Y. Huang, L. Zhang, Y. Shao, and Y. Wang, "High-sensitivity gas pressure sensor based on hollow-core photonic bandgap fiber Mach-Zehnder interferometer," Opt. Express, vol. 26, no. 23, p. 30108, 2018.

[44]S. Azad, E. Sadeghi, R. Parvizi, A. Mazaheri, and M. Yousefi, "Sensitivity optimization of ZnO clad-modified optical fiber humidity sensor by means of tuning the optical fiber waist diameter," Opt. Laser Technol., vol. 90, pp. 96-101, 2017.

[45]G. Wang, J. Dai, and M. Yang, "Fiber-optic hydrogen sensors: a review," IEEE Sens. J., vol. 21, no. 11, pp. 12706-12718, 2020.